Supporting Material

"Stochastic Model-Assisted Development of Efficient Low-Dose Viral Transduction in Microfluidics"

Camilla Luni[1,2,*], Federica Michielin[1,2,*], Luisa Barzon[3], Vincenza Calabrò[4], Nicola Elvassore[1,2]

[1]DII - Department of Industrial Engineering, University of Padova, Via Marzolo 9, 35131 Padova, Italy; telephone: +39-049-8275469; fax: +39-049-8275461; e-mail: nicola.elvassore@unipd.it

[2]VIMM - Venetian Institute of Molecular Medicine, Via Orus 2, 35129 Padova, Italy

[3]Department of Molecular Medicine, University of Padova, Via Gabelli 63, 35121 Padova, Italy

[4]Department of Engineering Modeling, University of Calabria, Via P. Bucci, 87036 Arcavacata di Rende (CS), Italy

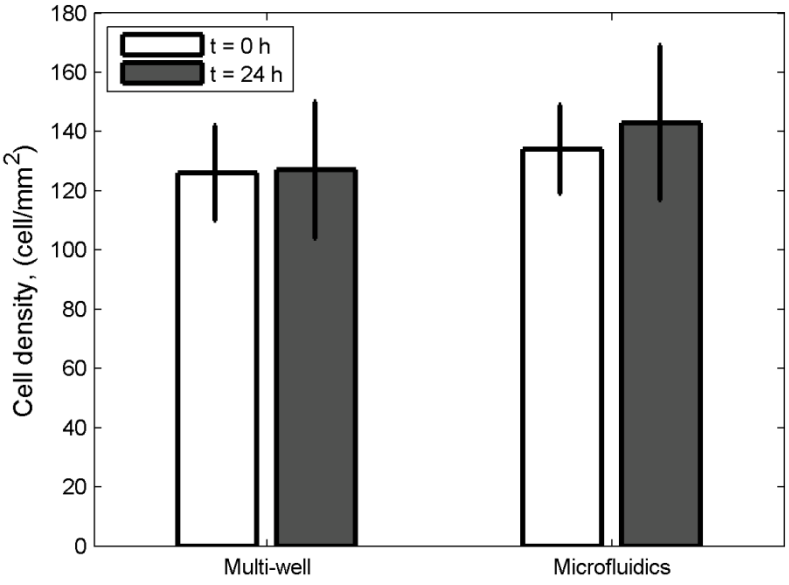

Figure S1. Cell density in the static multi-well plate system and in the microfluidic cell culture. Two time points are shown: t = 0 h, which represents the beginning of the infection process, and t = 24 h. Data are presented as mean ± standard deviation of 6 parallel experiments.

Description of virus entrance into a cell in the stochastic model.

Virus entrance into the cells is described in the model as a partially adsorbing boundary condition at $y = 0$, because not all cell-virus contacts are successful for introducing the virus into the cell. Thus, whenever the i-th virus during the time span Δt hits a cell ($y_i = 0$), it is adsorbed with probability $P_1\sqrt{\Delta t}$, and reflected otherwise.

Because of the solution scheme adopted (Eq. 1 in the main text), virus positions are simulated at discrete time points, separated by Δt. As time intervals are not infinitesimal, it is improbable to catch the exact time point when a virus hits a cell ($y_i(t+\Delta t) = 0$). Thus, given a virus in position $y_i(t) > 0$, two situations can occur after simulating the time interval Δt by Eq. (1), recalling that $\xi_{y,i}$ can be negative (it is a random variable having zero mean and unit variance):

- $y_i(t+\Delta t) < 0$. While physically unfeasible, this result implies that at an intermediate instance between t and $t+\Delta t$, y_i was zero and the virus hit the boundary. Thus, whenever $y_i(t+\Delta t) < 0$, the virus is either adsorbed into a cell with probability $P_1\sqrt{\Delta t}$ or reflected;
- $y_i(t+\Delta t) > 0$. On the other hand, even if the virus has a positive y_i coordinate at the end of the simulated interval, during its random walk it could have hit the surface at an intermediate time point between t and $t+\Delta t$. This event has a probability of occurrence given by $\exp\left[-y_i(t)\cdot y_i(t+\Delta t)/(D\cdot\Delta t)\right]$, as described in (33). Thus, the probability of virus entrance into a cell is given by the product of the two probabilities: $P_1\sqrt{\Delta t}\cdot\exp\left[-y_i(t)\cdot y_i(t+\Delta t)/(D\cdot\Delta t)\right]$.

Effect of MOI on spatial heterogeneity in microfluidics.

As reported in the main text, we verified with the simulations that cells located close to the inlet are more infected because exposed to a higher viral concentration. On the contrary, downstream, the actual virus concentration is less than that at the entrance and a gradient of infection levels develops along the channel. We performed a computational study of the effect of MOI on spatial heterogeneity under continuous perfused conditions in the microfluidic channel. A more drastic effect of virus depletion along the channel is visible at lower MOIs. For example, at instantaneous MOI 1, cells located near the channel outlet result 60% less infected than those near the inlet (Figure S2).

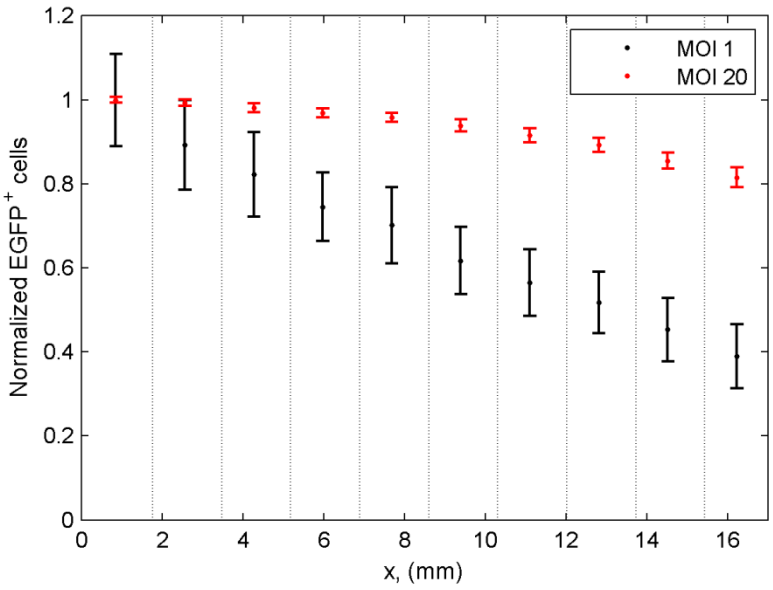

Figure S2. Computational study of spatial heterogeneity in the microfluidic system as a function of MOI. Stochastic simulation results of continuous channel perfusion with a flow rate of 0.1 μL/min for 90 min at the instantaneous MOIs indicated in figure legend. The percentage of $EGFP^+$ cells in each of the 10 equal sectors of the channel, indicated by the dotted lines, is shown after normalization by its value in the first sector. Error bars indicate mean ± standard deviation of the 100 simulations performed. Cell concentration is 130 cell/mm^2.

Heterogeneity, in terms of percentage of $EGFP^+$ cells, decreases at MOI 20 (Figure S2), and even more at MOI 50 where almost all cells are infected (Figure S3 A). However, heterogeneity in culture due to continuous perfusion in the channel is still present also at high MOI in terms of number of viruses per cell. Cells close to the inlet receive a higher number of viruses and a gradient is developed along the channel, as shown in Figure S3 B.

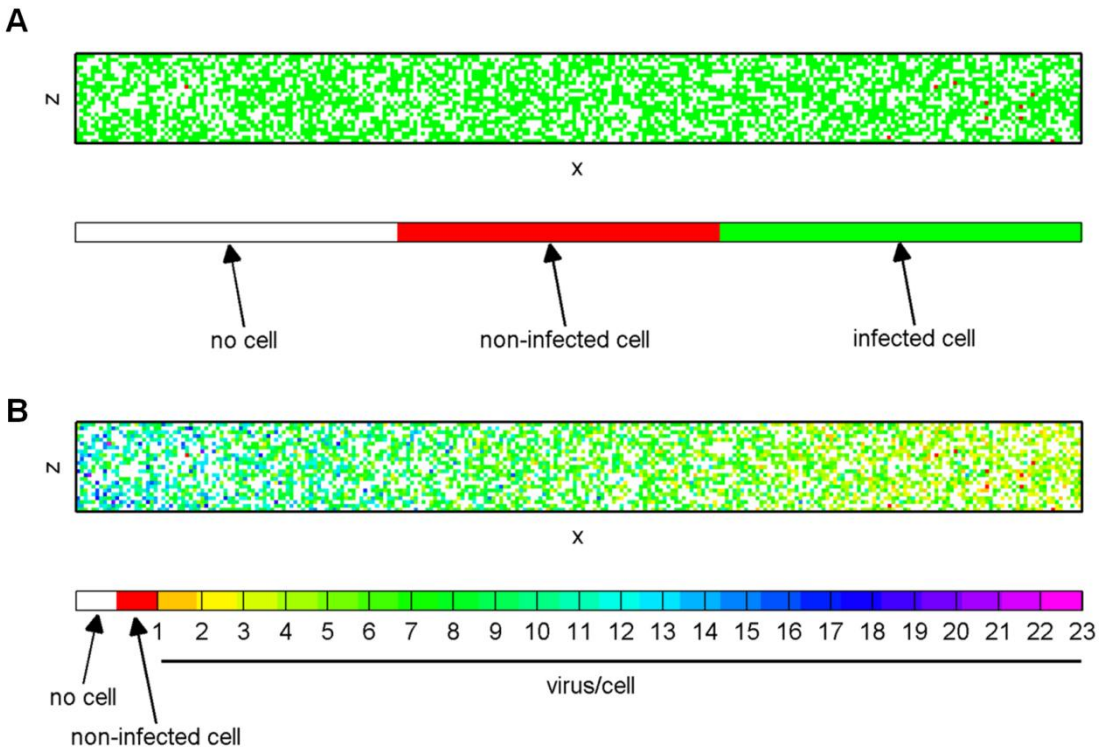

Figure S3. Computational study of spatial heterogeneity in the microfluidic system at high MOI. Representative results from a stochastic simulation of continuous channel perfusion with a flow rate of 0.1 μL/min for 90 min at an instantaneous MOI of 50. The bottom of the same microfluidic channel is represented in **A** and **B**, color legends are shown in the two cases. Flow direction is from left to right. Cell concentration is 130 cell/mm^2.

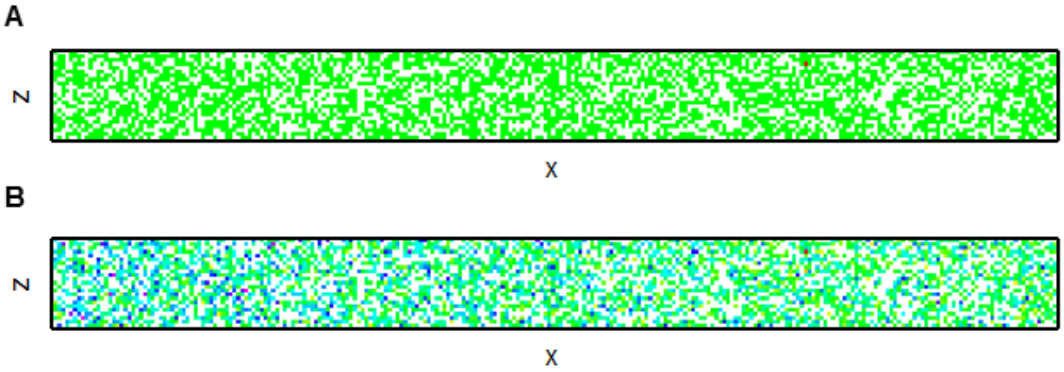

Figure S4. Computational study of spatial heterogeneity in the microfluidic system at high flow rate. Representative results from a stochastic simulation of continuous channel perfusion with a flow rate of 0.5 μL/min for 90 min at an instantaneous MOI of 50. The bottom of the same microfluidic channel is represented in **A** and **B**, color legends are reported in Figure S3. Flow direction is from left to right. Cell concentration is 130 cell/mm^2.

Simulations of EGFP protein production.

A direct comparison between model results, given by the number of virus per cell, and experimental measurements, in terms of cell fluorescence intensity, requires the insertion into the model of an additional module to describe viral DNA transcription and translation, together with EGFP RNA and protein degradation. While viruses enter cells in low copy number and thus require a stochastic modeling approach, the number of RNA and protein molecules per cell is much higher (about a hundred and a thousand, respectively) and is reasonably approximated by a deterministic approach.

We integrated our stochastic model with a simplified deterministic model, taken from the literature (1), given by an ODE system of two equations:

$$\begin{cases} \dfrac{d[R]}{dt} = k_{pr,R} \cdot n - k_{deg,R} \cdot [R] \\ \dfrac{d[P]}{dt} = k_{pr,P} \cdot [R] - k_{deg,P} \cdot [P] \end{cases} \quad \text{(S1)}$$

where n, $[R]$, and $[P]$ represent the concentration of viral DNA, RNA and protein in the cell; $k_{pr,R}$ and $k_{pr,P}$ the kinetic constants of RNA and protein production; and $k_{deg,R}$ and $k_{deg,P}$ the kinetic constants of RNA and protein degradation. The first equation describes EGFP RNA production and degradation, and the second accounts for the balance between EGFP protein production and degradation. Parameter values were taken from (1) and are also reported in Table S1.

Cell fluorescence intensity, f, was linearly correlated to protein concentration, $[P]$, according to the following expression:

$$[P] = \alpha \cdot f + \beta . \quad \text{(S2)}$$

where α and β are parameters, whose values, given in Table S1, were obtained by least square fitting of the experimental curve obtained 24 h and 36 h after the infection at MOI 5 shown in Figure 7D.

Table S1. Values of parameters in ODE system (S1) and equation (S2).

Parameter	Value	Unit
$k_{pr,R}$	$5.5 \cdot 10^{-4}$	s^{-1}
$k_{deg,R}$	$3.8 \cdot 10^{-5}$	s^{-1}
$k_{pr,P}$	$2.8 \cdot 10^{-4}$	s^{-1}
$k_{deg,P}$	$1.4 \cdot 10^{-5}$	s^{-1}
α	7.26	$\frac{\text{no. molecule/cell}}{\text{fluorescence a.u.}}$
β	53.19	no. molecule/cell

A comparison between model simulation results and experimental data is reported in Figure S5, in terms of complementary cumulative distribution of fluorescence intensity in the cell population. The simulations well reproduce the experimental distributions for four infections at MOI 5 and the first time points for two infections at MOI 10. The results are especially encouraging considering that the added module for RNA and protein balances is taken from a model in the literature without changes in its structure or parameter values. However, the model overestimates the quantity of EGFP protein produced after one infection at MOI 20. Further experimentation would be needed to explore the sources of these differences, and a more detailed mathematical model that accounts in detail for phenomena such as intra-cellular cell-virus interactions.

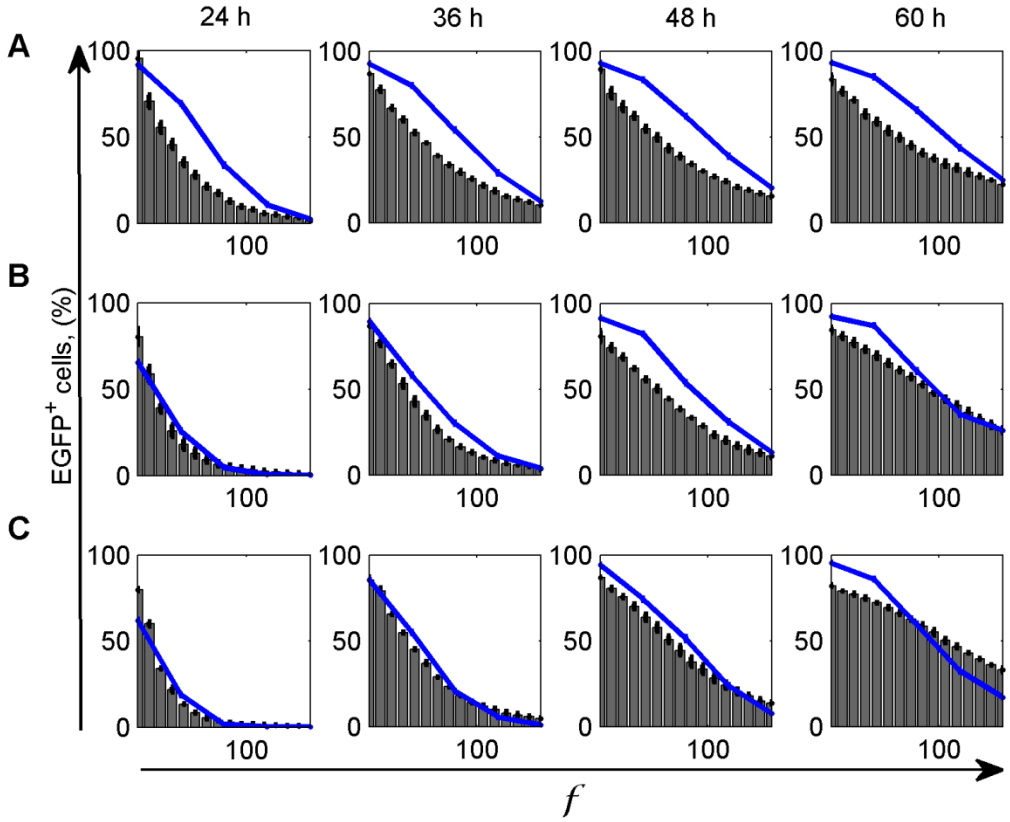

Figure S5. Comparison of experimental data and model simulations of EGFP fluorescence intensity in the cell population after multiple viral transductions within the microfluidic platform. Complementary cumulative distributions obtained from experimental data, shown as gray bars (same data reported in Figure 7D), and simulation results, represented by blue lines, at the following conditions: one infection at MOI 20 (A), two infections at MOI 10 (B), and 4 at MOI 5 (C). Error bars indicate mean ± standard deviation of experiments repeated twice and of 100 simulations performed, respectively.

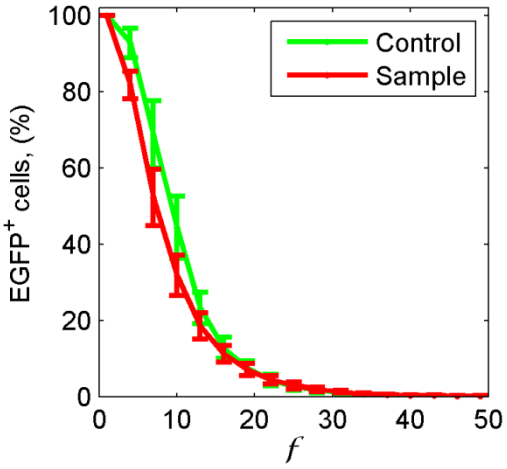

Figure S6. Test of virus adsorption on the walls of the microfluidic system.

We separately infected cells seeded at the same confluence in a microfluidic platform with two different virus-containing media: the control with medium kept in a 1.5 mL tube for 2 h at 37°C and 5% CO2; and the sample with medium previously injected inside microfluidic channels without cells for 2 h. In both cases MOI 20 was used. After 24 h from infection, we compared the efficiency of infection in the cell populations treated with the two different media. Fluorescence analysis was used to quantify the percentage of $EGFP^+$ cells inside the microfluidic channels as previously described.

Data are shown as mean ± standard deviation of 4 parallel experiments. We compared the cumulative distributions of fluorescence in the cell populations by a Kolmogorov-Smirnov test. No significant difference was detected (p-value <0.01). Thus, virus losses due to binding to the surfaces of the microfluidic channels are negligible and within the experimental variability of the system.

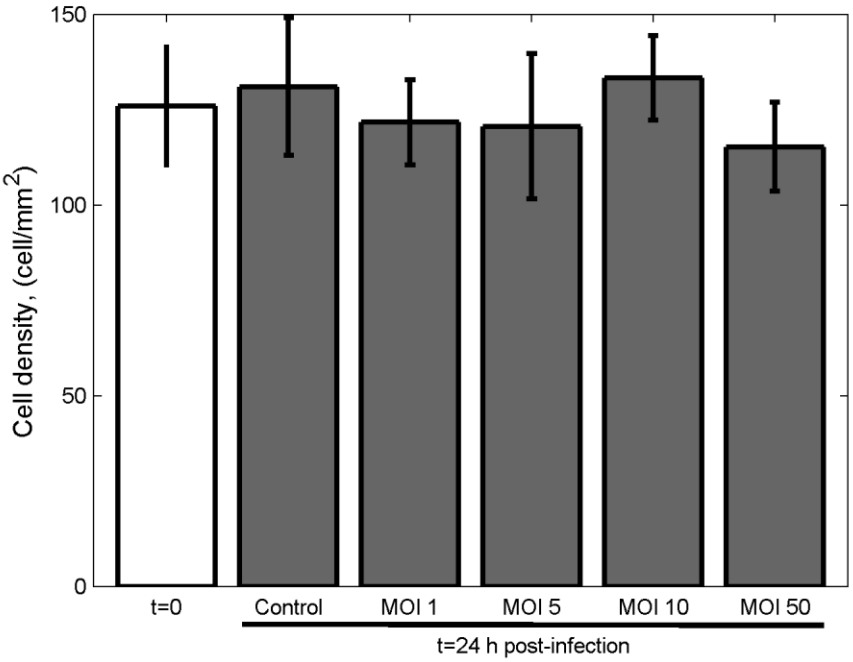

Figure S7. Effect of MOI on cell viability in a multi-well plate.

We infected cells seeded at 130 cell/mm^2 in a 24-well tissue culture plate at the indicated MOIs for 4 hours. Cell count was performed at t = 0 h, immediately before the infection process, and at t = 24 h. The control wells were treated as the others, but using virus-free medium during the infection step. We verified that cell death was negligible in all the wells. Data are presented as mean ± standard deviation of 3 parallel experiments. Cell densities were compared using one-way ANOVA with Tukey post-test, with $p<0.05$ indicating significance. Each pair comparison with *t=0* and *Control* densities did not show significant differences, demonstrating that viral concentration does not affect cell viability up to MOI 50 in these experimental conditions.

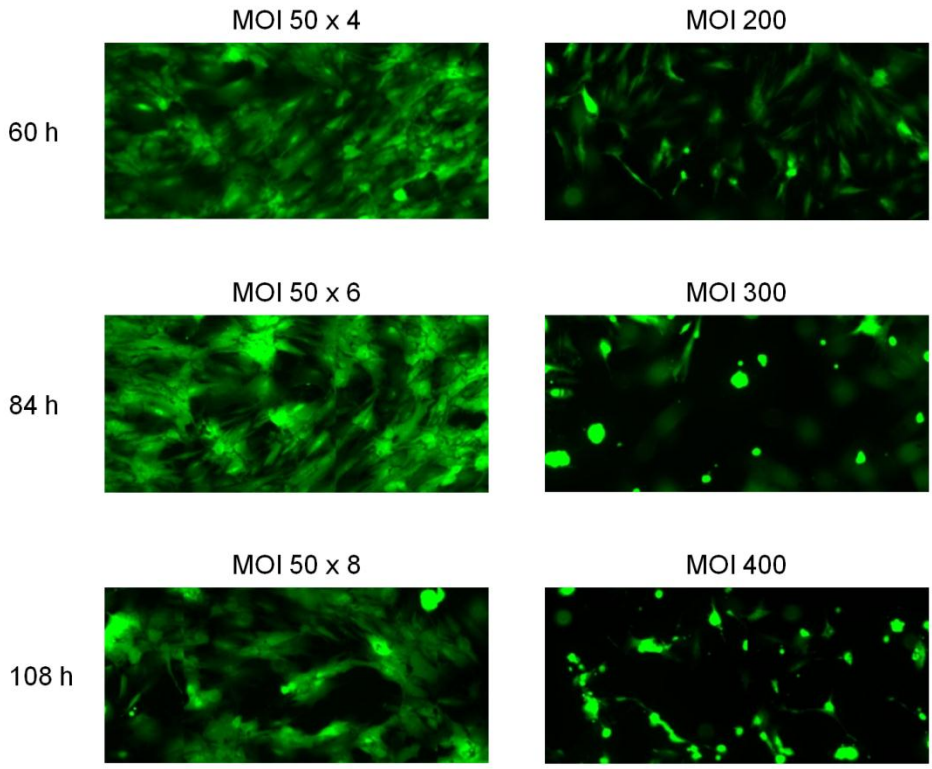

Figure S8. Single vs. multiple pulses of viral transduction.

We separately infected cells seeded at the same confluence in a microfluidic platform with different viral concentrations: MOI 200, 300 and 400 for a single infection at time 0; MOI 50 repeated every 12 h for 4, 6, and 8 times, starting at time 0. Images (10X) were taken 24 h after the last infection in the multiple-infection channels. Microscope exposure was changed at different time points to avoid signal over-saturation, but it is kept constant for the two images at the same time point. Data are representative of 2 parallel experiments.

High mortality is evident for a single infection at high MOI, especially at MOI 300 and 400. On the other hand, the multiple-infection strategy allows higher EGFP expression with reduced cell loss, although at MOI 50 x 8 some virus toxicity is present also in this condition.

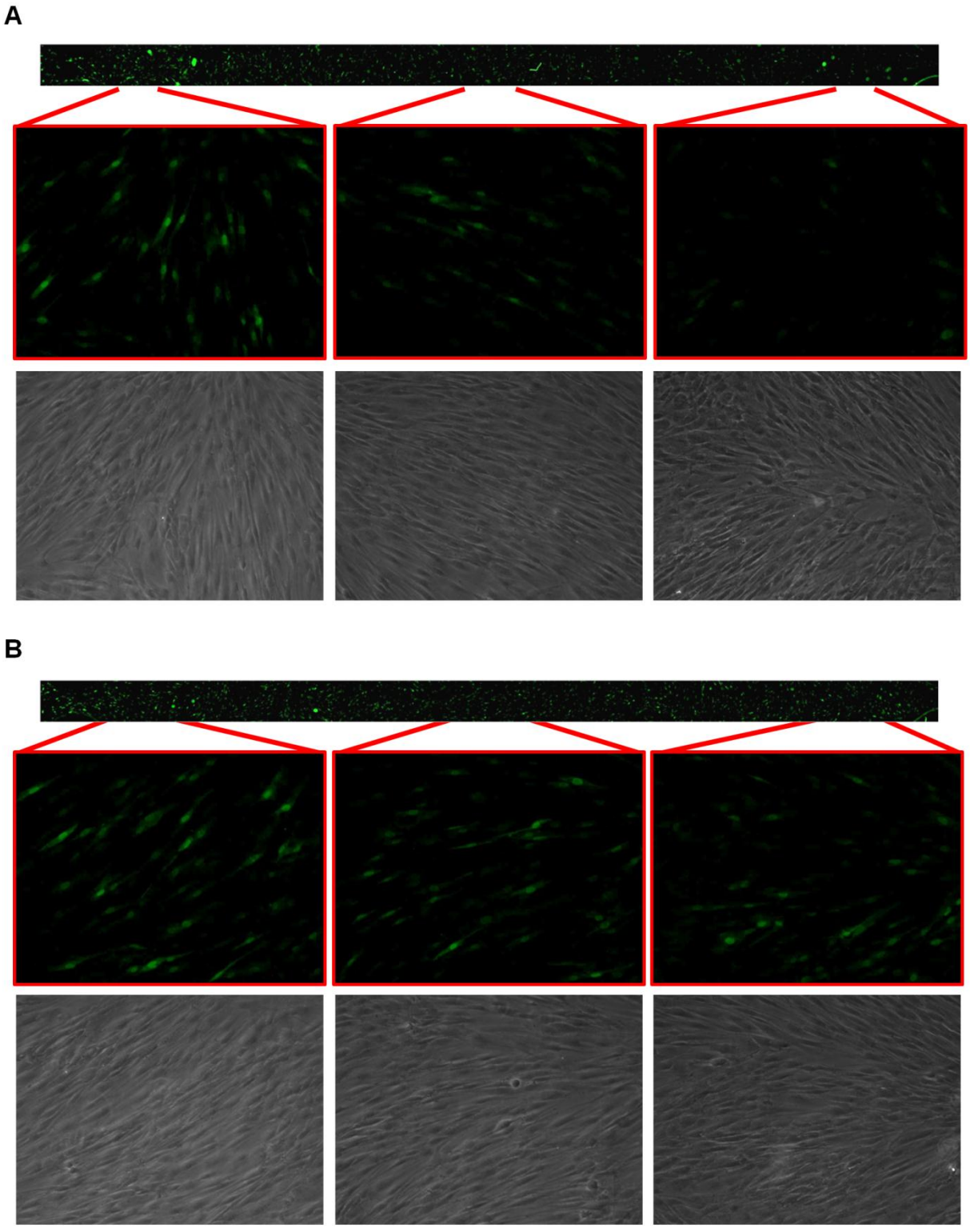

Figure S9. Continuous vs. discontinuous channel perfusion. (A) Experimental results of continuous channel perfusion with a flow rate of 0.1 μL/min for 90 min. (B) Experimental results of discontinuous perfusion: 2 min of inflow at 6 μL/min, 90 min without perfusion, and 2 min of

outflow at 6 μL/min. Images of the whole channel (10X) and of single parts of the channel (20X) were taken 24 h after the infection. Image enhancement was performed identically for the images in A and B. Cell seeding concentration was 200 cell/mm^2, instantaneous MOI 5, flow direction in the channels from left to right.

Supporting References

1. Dinh, A. T., T. Theofanous, and S. Mitragotri. 2005. A model for intracellular trafficking of adenoviral vectors. Biophys J 89:1574-1588.